

Improving Computed Tomography (CT) Reconstruction via 3D Shape Induction

Elena Sizikova

New York University

ES5223@NYU.EDU

Xu Cao

New York University

XC2057@NYU.EDU

Ashia Lewis

The University of Alabama

ATLEWIS5@CRIMSON.UA.EDU

Kenny Moise

Université Quisqueya

KENNY.MOISE@UNIQ.EDU

Megan Coffee

NYU Grossman School of Medicine

MEGAN.COFFEE@NYULANGONE.ORG

Abstract

Chest computed tomography (CT) imaging adds valuable insight in the diagnosis and management of pulmonary infectious diseases, like tuberculosis (TB). However, due to the cost and resource limitations, only X-ray images may be available for initial diagnosis or follow up comparison imaging during treatment. Due to their projective nature, X-rays images may be more difficult to interpret by clinicians. The lack of publicly available paired X-ray and CT image datasets makes it challenging to train a 3D reconstruction model. In addition, Chest X-ray radiology may rely on different device modalities with varying image quality and there may be variation in underlying population disease spectrum that creates diversity in inputs. We propose shape induction, that is, learning the shape of 3D CT from X-ray without CT supervision, as a novel technique to incorporate realistic X-ray distributions during training of a reconstruction model. Our experiments demonstrate that this process improves both the perceptual quality of generated CT and the ac-

curacy of down-stream classification of pulmonary infectious diseases.

Keywords: CT; 3D Reconstruction; Analysis of Pulmonary Diseases

1. Introduction

This paper tackles the problem of 3D reconstruction of CT from X-ray images. The ability to visualize 3D internal anatomy allows medical professionals to better assess abnormal pulmonary findings, including those associated with infectious diseases, such as COVID-19 or TB. In particular, TB is a global infectious disease with 1.7 billion infected worldwide and over 1.5 million deaths a year, and is currently (as of 2022) second only to COVID-19 as an infectious cause of death annually.

In many rural and under-served populations, access to radiology is limited. X-rays, which are more accessible, do not provide the nuanced insight multiple slices of imaging a CT scanner provides. A single X-ray is cheaper and easier to obtain and hence may be the only accessible option, besides ultrasound. Even when CTs are available, fol-

low up with repeat CTs is not practical and would expose patients to unnecessary radiation. However, X-rays contain only a projected, noisy subset of the visual information present in CT, making it more challenging to identify certain pathological features. Additionally, there may not be enough radiologists and other clinicians present to interpret either the X-ray or the CT images in resource-limited settings. The lack of paired chest X-ray and CT datasets, the diversity of patient findings and image quality limitations make the task of learning generative CT models from X-ray inputs a particular challenge. On the other hand, for underserved populations, both an automatic technique for chest CT prediction and for diagnosis of pulmonary infectious disease would improve the quality and timely delivery of healthcare (Lewis et al., 2021).

In this work, we build upon the system proposed in X2CT (Ying et al., 2019) in several ways. In particular, this system trains on pairs of real CT images and X-rays generated synthetically using the digitally reconstructed radiograph (DRR) technology (Milickovic et al., 2000), due to the lack of available paired training data. To bridge the gap between real and synthetic input data distributions, CycleGAN (Zhu et al., 2017), an unpaired image translation pre-processing, is used. We observe that this image pre-processing step introduces noise and degrades the quality of input X-rays. In addition, available real X-ray images are not used to improve the expressiveness of the CT generative model. We therefore propose to use shape induction (Gadelha et al., 2017) as a strategy to address these limitations. Inspired by average intensity projection (AIP) and ray summation (Dalrymple et al., 2005), we introduce a shape induction step: when the generative model is presented with an example of an X-ray image without a corresponding CT, the system

evaluates whether the projected X-ray obtained from a predicted CT image matches the input X-ray (see Figure 1). This allows us to incorporate any input X-ray datasets directly during training of the CT generative model. We find that the CT images created by our system are more predictive of disease and better capture diversity in clinical radiology findings. Through this work, we highlight the challenge of capturing image variability in automatic techniques for generative modeling and classification in medical imaging, and show how unsupervised shape induction can benefit healthcare accessibility in low-resource healthcare settings.

CT and X-rays use the same imaging technique but different actual machines. CTs are standardly only available in high resource tertiary medical settings; X-rays can be available in rural, low resource settings, cost less, create less radiation exposure, and can be done at bedside. CT is preferred by clinicians because it provides more detailed imaging which is intuitively comprehensible and mirrors the lungs anatomically. Moving between successive image slices when reading a CT, one can show the cavities and nodules that would be obscured in a single image where findings would overlap. By reconstructing CTs from X-rays, clinicians can provide more targeted clinical care, train with this imaging technology otherwise potentially inaccessible in low resource settings, and improve their understanding of TB, benefiting their patients overall. On the other hand, automatic classification streamlines screening of many images, saving clinician/patient wait times and reduces risk of missing infectious TB cases. Our contributions are as follows. (1) We propose to train an X-ray-to-CT reconstruction model with shape induction, which allows learning from X-ray images only, without CT annotation. (2) We show that the CT images from a model trained with shape induction

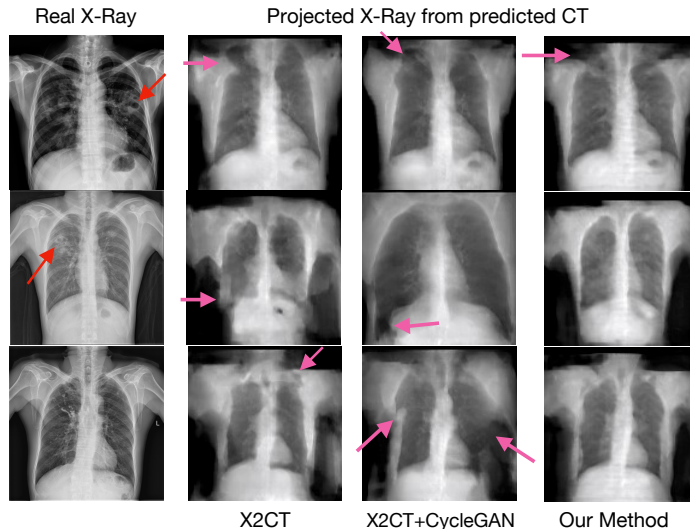


Figure 1: Visualization of real X-rays from the TBX11K (Liu et al., 2020) dataset, as well as the corresponding original and fine-tuned projections from predicted CT images. We find that our proposed method better captures anatomical details, such as the shape of the lung and the pleural and thoracic integrity, avoiding gaps in the thoracic wall and pleural membrane surrounding the lungs seen on the projected X-rays and their corresponding generated CTs (not shown). The red arrow identifies the pulmonary abnormalities in the lung fields bilaterally which likely corresponds to TB and is lost in the projected images. The pink arrows show where there are gaps in the thoracic wall and pleura, which normally separate the lungs from the outside world, but here the lungs are imaged as continuous with the space outside the body. These unrealistic findings, not seen in the real X-rays, were less common in our method.

more accurately classify TB by up to 6.46% and better capture diversity in the underlying patient pulmonary findings, as judged by a medical professional¹.

2. Approach

Let $B^{CT} = \{b_1^{CT}, b_2^{CT}, \dots, b_n^{CT}\}$ be a dataset of real CT images. Using the digitally reconstructed radiograph (DRR) mapping g , one can obtain a set of realistic, synthetic images $\hat{G} = \{\hat{g}_1, \hat{g}_2, \dots, \hat{g}_n\}$ such that $\hat{g}_i = g(b_i^{CT})$ for $i = 1, 2, \dots, n$. Let G and D be a gener-

ator and a discriminator, respectively, that map the distribution of X-ray images to their corresponding CT image counterparts. In X2CT (Ying et al., 2019), G and D are trained using the LSGAN (Mao et al., 2017) training process. Specifically, G is optimized using a combination of the following objectives.

The first objective is the adversarial loss $L_{LSGAN} := \frac{1}{2}E[(D(G(x)|x) - 1)^2]$, where $x \sim d_{\hat{G}}$ and $d_{\hat{G}}$ is the distribution of X-rays generated using DRR. The L_{LSGAN} objective encourages the output CT to be realistic. The second objective is the reconstruction loss $L_{re} := \|y - G(x)\|_2^2$, which

1. Our code is available at: https://github.com/esizikova/medsynth_public

measures the MSE between each GT CT b_i^{CT} and its estimate $\hat{b}_i^{CT} = G(\hat{g}_i)$. The third objective is the projection loss $L_{pl} := \frac{1}{3} \sum_{i=1,2,3} \|(Proj_i(y) - Proj_i(G(x)))\|_1$, where $Proj_{1,2,3}$ are the axial, coronal, and sagittal plane projections, respectively, and $\|\cdot\|_1$ is the L_1 distance. L_{pl} encourages the 2D projections of b_i^{CT} , the GT CT, and $G(\hat{g}_i)$, the predicted CT, to match.

In practice, the real X-ray distribution p_{data} may not match the DRR X-ray distribution $d_{\hat{G}}$. Therefore, (Ying et al., 2019) proposes to use an image translation approach to map each realistic input $x \sim p_{data}$ to its DRR-style version $\hat{x} = s(x)$, where s is a learnt function. Therefore, the CT corresponding to x will be approximated using $G(\hat{x})$, making the assumption that $x \approx \hat{x}$. In our work, we argue that s may lose information about x , i.e., $x \not\approx \hat{x}$, and propose to learn G jointly on both p_{data} and $d_{\hat{G}}$, using shape induction, described below.

Shape Induction Let $D^X = \{d_1^X, d_2^X, \dots, d_m^X\} \sim p_{data}$ be a dataset of real X-ray images (data points in B^{CT} and D^X are independent, and typically collected from different patients). Given an X-ray x and its predicted CT image $G(x)$, the coronal projection $Proj_1(G(x))$ is a ray sum estimate, whose appearance is similar to the input X-ray (Dalrymple et al., 2005). Based on this observation, our key idea is to define a new shape induction loss function, $L_{sind} := \|Proj_2(G(x)) - x\|_2^2$, where $x \sim p_{data}$. L_{sind} measures, via MSE, whether the appearance of the real X-ray and its projected version from the predicted CT match. Notice that L_{sind} does not require the presence of ground truth CT corresponding to x .

We train G using a combined, weighted total loss function $L_G := \lambda_1 L_{LSGAN} + \lambda_2 L_{re} + \lambda_3 L_{pl} + \lambda_4 L_{sind}$. D is trained using the standard LSGAN discriminator loss (please see (Ying et al., 2019)).

3. Experimental Details

We evaluate our approach on the public dataset TBX11K (Liu et al., 2020). We use the official data split in (Liu et al., 2020) that also includes multiple smaller, public sets (Jaeger et al., 2014; Chauhan et al., 2014). For qualitative performance evaluation, we evaluate on COVID-19-CT-CXR (Peng et al., 2020) subset that consists of paired X-ray and CT images of patients from COVID-19 articles in the PubMed Central Open Access (PMC-OA). The images considered in this experiment are pathological examples cropped from COVID-19 articles in the PubMed Central Open Access (PMC-OA). For example, they include annotations, such as figure numbers ‘‘A’’ and ‘‘B’’ in the first line of Figure 2, which our model was not trained on. Due to the nature of the dataset and the image collection process, these images are a difficult test set for our system. Two board-certified medical professionals evaluated and commented on the visual artifacts found in both X-rays and CTs.

4. Results

In this section, we present qualitative and quantitative results of our method. For quantitative evaluation of clinical correctness, we measure if the generated images can predict the presence of TB.

Comparison of CT Generation Strategies In Table 1, we compare the CT images generated using different training strategies on the task of classification into healthy, sick, and TB. We find that the proposed method trained with shape induction obtains both the highest classification accuracy and the best recall of TB examples. On the other hand, we find that the cycleGAN (Zhu et al., 2017) CT offers less prediction value, with lower classification scores and lower TB recall rates. This is because cycleGAN (Zhu

	X2CT (Ying et al., 2019)	X2CT+CycleGAN (Zhu et al., 2017)	Our Method
Classification Accuracy	0.925±0.003	0.882±0.005	0.939±0.003
TB Recall	<u>0.789±0.008</u>	0.693±0.038	0.826±0.006
TB Precision	<u>0.915±0.019</u>	0.866±0.021	0.934±0.008

Table 1: Quantitative comparison across different CT generation techniques. Our method (using shape induction) obtains best results. Best result is in bold and the second best is underlined.

et al., 2017) limits the expressiveness of X-rays, normalizing clinical abnormalities, and adds noise (see Appendix).

Qualitative Comparison of Real and Predicted CT Images In Figure 2, we visualize the input X-rays, ground truth and predicted CT images from the COVID-19-CT-CXR (Peng et al., 2020) dataset. The images in this dataset are obtained from scraping public articles and depict pulmonary findings of severe COVID-19 and other respiratory diseases, therefore, presenting a particularly challenging case for our algorithm. Compared to the X2CT (Ying et al., 2019) and X2CT+CycleGAN (Zhu et al., 2017), our model captures more anatomic details of the CT images.

5. Limitations

The model described in this paper presents some limitations. In many instances, it failed to capture basic anatomic features, such as the integrity of the chest wall. It developed aberrant anatomic structures such as three lungs on CT in other cases. In other instances, while capturing basic anatomy, it failed to detect pulmonary findings on CT while they are present on X-rays. Therefore, the model did not create the ideal CT for clinical use with every output. When comparing classification based on X-rays and generated CT, we did not observe a consistent improvement in classification performance using the generated CT. We assess our approach qualitatively and via a proxy task (classification), and while evaluation

using image reconstruction metrics such as SSIM/L2 would be more preferable, this approach would require paired X-ray and CT data, which is unavailable for our application. Further evaluation is necessary to ensure that our evaluation is not susceptible to shortcut learning, for example, that the decision of classification model decisions are based on reconstructions of clinically relevant pathologies.

The model has also been run on a relatively low number of input X-rays which are not able to encompass the full diversity of findings in pulmonary TB, let alone the wider range of disease in pulmonary images. Moreover, the datasets used here did not include the lower-quality images often relied upon in resource-limited settings, especially where digital X-rays are not available and plain films are used. These databases are also not representative of the populations where TB is more common. In areas where TB is more frequent, patients present more commonly with a primary infection, more frequently at a younger age, accessing care with more advanced disease, than in populations where the disease is less common and often due to reactivation of past disease in older adults, and may have different lung findings, and can access care and imaging earlier before more substantial lung pathology develops. HIV can lead to TB manifesting with few radiographic findings and images would need to be compared to a more varied backdrop of other pulmonary disease findings as a wide range of opportunistic infections are

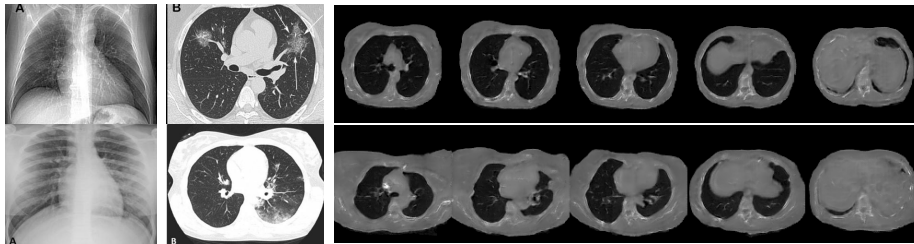


Figure 2: Qualitative comparison of CT generated from ground truth X-rays and corresponding real CT images obtained from the COVID-19-CT-CXR (Peng et al., 2020) dataset (images from (Schmitt and Marchiori, 2020; Musolino et al., 2020)). While all three methods exhibit significant artifacts, we find that the proposed technique is better at a) capturing some of the abnormalities associated with disease without over-sanitizing and b) avoiding anatomical abnormalities (thoracic wall defects) not consistent with Chest X-rays, as seen with other methods.

common in those with HIV, but not those who are HIV negative.

6. Conclusion and Future Work

In this work, we present an approach for training an automatic chest CT reconstruction algorithm with X-ray only. We augment existing model training on DRR-generated X-ray and CT pairs with a shape induction loss, allowing the model to learn from only real input X-rays. This approach allows learning the variability of real X-ray images and directly incorporating it into the training of the CT generation model. The ability to learn rich distributions from real X-rays is particularly important for practical applications where there is a need to adapt to different imaging sensor types and anatomies.

In future work, it will be important to devise techniques to constrain the model to generate more realistic outputs and ensure the model is not generating sanitized CT images without the abnormalities representing disease processes. Clearly representing abnormal lung findings would help clinicians identify the type of illness (such as TB) and features of this illness which may affect man-

agement (may need fluid drainage, may have lifelong damage). At the same time, it is important that the CT images do not misrepresent findings and show gross and erroneous abnormalities (e.g., chest wall gaps, additional lungs) not consistent with these patients being alive and hence would decrease the trust in the tools by clinicians using the tool. In addition, it would be extremely valuable to design a system that would focus on capturing and identifying distinct lung findings indicative of TB, including cavities, apical capping, micronodules of miliary TB, as well as features often shared with other diseases, like infiltrates and fluid collecting in pleural space (pleural effusion). Further model development will require expansion of existing databases to more robustly represent the TB populations where disease is often more severe at time of imaging, and may include different types of findings seen in younger patients with initial exposures to TB. Overall, this work is a step towards developing a tool which can classify types of pulmonary disease, including TB and its specific subtypes, as well as provide clinicians with CT imaging after obtaining only chest X-rays.

References

- Yosra M Alkabab, Mushira A Enani, Nouf Y Indarkiri, and Scott K Heysell. Performance of computed tomography versus chest radiography in patients with pulmonary tuberculosis with and without diabetes at a tertiary hospital in Riyadh, Saudi Arabia. *Infection and drug resistance*, 2018.
- Samuel G Armato III, Geoffrey McLennan, Luc Bidaut, Michael F McNitt-Gray, Charles R Meyer, Anthony P Reeves, Binsheng Zhao, Denise R Aberle, Claudia I Henschke, Eric A Hoffman, et al. The lung image database consortium (LIDC) and image database resource initiative (IDRI): a completed reference database of lung nodules on CT scans. *Medical Physics*, 2011.
- Joshua Burrill, Christopher J Williams, Gillian Bain, Gabriel Conder, Andrew L Hine, and Rakesh R Misra. Tuberculosis: a radiologic review. *Radiographics*, 2007.
- L Caponetti and AM Fanelli. 3D Bone reconstruction from two X-ray views. In *EMBS*, 1990.
- Arun Chauhan, Devesh Chauhan, and Chittaranjan Rout. Role of gist and PHOG features in computer-aided diagnosis of tuberculosis without segmentation. *PLoS one*, 2014.
- Dongdong Chen, Julián Tachella, and Mike E Davies. Equivariant imaging: Learning beyond the range space. In *ICCV*.
- Neal C Dalrymple, Srinivasa R Prasad, Michael W Freckleton, and Kedar N Chintapalli. Introduction to the language of three-dimensional imaging with multidetector CT. *Radiographics*, 2005.
- Kunio Doi. Computer-aided diagnosis in medical imaging: historical review, current status and future potential. *Computerized medical imaging and graphics*, 2007.
- Alexey Dosovitskiy, Lucas Beyer, Alexander Kolesnikov, Dirk Weissenborn, Xiaohua Zhai, Thomas Unterthiner, Mostafa Dehghani, Matthias Minderer, Georg Heigold, Sylvain Gelly, et al. An image is worth 16x16 words: Transformers for image recognition at scale. In *ICLR*, 2020.
- Linh T. Duong, Nhi H. Le, Toan B. Tran, Vuong M. Ngo, and Phuong T. Nguyen. Detection of tuberculosis from chest X-ray images: Boosting the performance with vision transformer and transfer learning. *Expert Systems with Applications*, 2021.
- Matheus Gadelha, Subhansu Maji, and Rui Wang. 3D shape induction from 2D views of multiple objects. In *3DV*, 2017.
- Philipp Henzler, Niloy J Mitra, and Tobias Ritschel. Escaping plato’s cave: 3d shape from adversarial rendering. In *ICCV*, 2019.
- Philipp Henzler, Volker Rasche, Timo Ropinski, and Tobias Ritschel. Single-image Tomography: 3D Volumes from 2D Cranial X-Rays. In *CGF*, 2018.
- Phillip Isola, Jun-Yan Zhu, Tinghui Zhou, and Alexei A Efros. Image-to-image translation with conditional adversarial networks. In *CVPR*, 2017.
- Stefan Jaeger, Sema Candemir, Sameer Antani, Yi-Xiang J Wang, Pu-Xuan Lu, and George Thoma. Two public chest x-ray datasets for computer-aided screening of pulmonary diseases. *Quantitative imaging in medicine and surgery*, 2014.
- Yoni Kasten, Daniel Doktofsky, and Ilya Kovler. End-to-end convolutional neural network for 3D reconstruction of knee

- bones from bi-planar X-ray images. In *MLMIR*, 2020.
- Jinsa Kuruvilla and K Gunavathi. Lung cancer classification using neural networks for CT images. *Computer methods and programs in biomedicine*, 2014.
- Ashia Lewis, Evanjelin Mahmoodi, Yuyue Zhou, Megan Coffee, and Elena Sizikova. Improving tuberculosis (TB) prediction using synthetically generated computed tomography (CT) images. In *CVPRW*, 2021.
- Yun Liu, Yu-Huan Wu, Yunfeng Ban, Huifang Wang, and Ming-Ming Cheng. Rethinking computer-aided tuberculosis diagnosis. In *CVPR*, 2020.
- Halgurd S Maghdid, Aras T Asaad, Kayhan Zrar Ghafoor, Ali Safaa Sadiq, Seyedali Mirjalili, and Muhammad Khuram Khan. Diagnosing COVID-19 pneumonia from X-ray and CT images using deep learning and transfer learning algorithms. In *Multimodal Image Exploitation and Learning*. International Society for Optics and Photonics, 2021.
- Xudong Mao, Qing Li, Haoran Xie, Raymond YK Lau, Zhen Wang, and Stephen Paul Smolley. Least squares generative adversarial networks. In *ICCV*, 2017.
- Natasa Milickovic, Dimos Baltas, S Gianoulis, M Lahanas, and N Zamboglou. CT imaging based digitally reconstructed radiographs and their application in brachytherapy. *Physics in Medicine & Biology*, 2000.
- Anna Maria Musolino, Maria Chiara Supino, Danilo Buonsenso, Valentina Ferro, Piero Valentini, Andrea Magistrelli, Mary Haywood Lombardi, Lorenza Romani, Patrizia D’Argenio, Andrea Campana, et al. Lung ultrasound in children with COVID-19: preliminary findings. *Ultrasound in medicine & biology*, 2020.
- Yifan Peng, Yuxing Tang, Sungwon Lee, Yingying Zhu, Ronald M Summers, and Zhiyong Lu. COVID-19-CT-CXR: a freely accessible and weakly labeled chest X-ray and CT image collection on covid-19 from biomedical literature. *IEEE Transactions on Big Data*, 2020.
- Tuan D Pham. A comprehensive study on classification of COVID-19 on computed tomography with pretrained convolutional neural networks. *Scientific reports*, 2020.
- W Schmitt and E Marchiori. Covid-19: round and oval areas of ground-glass opacity. *Pulmonology*, 2020.
- Xingde Ying, Heng Guo, Kai Ma, Jian Wu, Zhengxin Weng, and Yefeng Zheng. X2CT-GAN: reconstructing CT from bi-planar x-rays with generative adversarial networks. In *CVPR*, 2019.
- Jun-Yan Zhu, Taesung Park, Phillip Isola, and Alexei A Efros. Unpaired image-to-image translation using cycle-consistent adversarial networks. In *ICCV*, 2017.
- Xiongfeng Zhu and Qianjin Feng. Mvc-net: Multi-view chest radiograph classification network with deep fusion. In *ISBI*, 2021.
- Hasib Zunair, Aimon Rahman, Nabeel Mohammed, and Joseph Paul Cohen. Uniformizing techniques to process CT scans with 3D CNNs for tuberculosis prediction. In *PRIME*, 2020.

	$\lambda_4 = 0.0$	$\lambda_4 = 0.1$	$\lambda_4 = 1.0$	$\lambda_4 = 10.0$	$\lambda_4 = 100.0$
Classification Accuracy	0.925 \pm 0.003	0.930 \pm 0.004	0.937 \pm 0.003	0.939\pm0.003	0.936 \pm 0.013
TB Recall	0.789 \pm 0.008	0.806 \pm 0.016	0.817 \pm 0.034	0.826\pm0.006	0.821 \pm 0.052
TB Precision	0.915 \pm 0.019	0.916 \pm 0.014	0.925 \pm 0.016	0.934 \pm 0.008	0.940\pm0.024

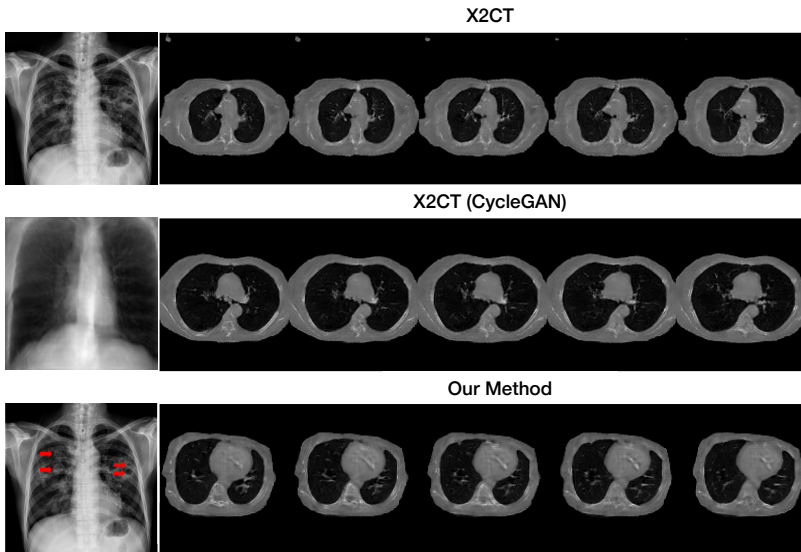
Table 2: Ablation study of λ_4 , weight influence of shape induction loss.

Figure 4: Comparison of CTs generated using different strategies.

CT classification, we use the 3D-CNN model previously proposed in (Zunair et al., 2020) for TB classification from CT. The performance of each model is averaged over three training runs. All experiments are performed in PyTorch using a single NVIDIA Quadro RTX8000 GPU with 100GB CPU memory cap.

Training Details For shape induction, we pre-train D and G for $n_e^1 = 90$ epochs, then alternate fine-tuning on D^X and B^{CT} for $n_e^2 = 10$ epochs. The baseline model (single-view X2CT (Ying et al., 2019)) is trained on B^{CT} only for $n_e = 100$ epochs. This model consists of a 2D encoder and a 3D decoder CNN with skip connections between the encoder and decoder. A 3D PatchGAN (Isola et al., 2017) discriminator is used for adversarial training. The X-Ray classification model is trained for $n = 50$ epochs, and the

best model according to the validation set is used for testing. The model consists of four convolutional blocks, followed by a global average pooling (GAP) layer and two fully connected layers, with number of outputs 512 and number of classes $K = 3$, respectively, with a dropout layer in between. The model is also trained for $n = 50$ epochs, and the best model, based validation, is used for testing. The CT reconstruction takes about 22 hours to train, the classification model takes about 5 hours (CT) and 1 hour (X-Ray).

Analysis of Shape Induction Influence

Based on the experiments in Table 2, we find that using larger shape induction weight λ_4 improves the generation of 3D CT. We compare the classification model using 3D CT generated by $\lambda_4 = 0$ (original X2CT mode), and $\lambda_4 = 0.1, 1.0, 10.0, 100.0$, and find that $\lambda_4 = 10.0$ achieves most accurate down-

stream CT classification model. We perform the ablation study and selected the optimal value of λ_4 based on the validation set ($\lambda_4 = 10.0$). Results in Table 2 reflect performance on the test set.

Visual Comparison of Generated CT

We report a visual comparison of CT generated using different strategies in Figure 4. CTs that use CycleGAN (Zhu et al., 2017) X-rays often exhibit less artifacts as the input X-rays are closer to the training distribution. On the other hand, the resulting CT images are less expressive and do not capture the abnormalities seen in the Chest X-rays which would be associated with TB. By using shape induction, we are able to maintain the generated image variability while matching the distributions in input X-rays. Here, red arrows pointing to pulmonary abnormalities are seen on the Chest X-ray and some abnormalities are seen on the CT images in the expected, corresponding location. These expected disease-associated abnormalities were not captured in the CycleGAN approach.

7. Acknowledgments

ES was supported by the Moore-Sloan Data Science Environment initiative (funded by the Alfred P. Sloan Foundation and the Gordon and Betty Moore Foundation) through the NYU Center for Data Science. AL was supported by the NYU Center for Data Science (CDS) Undergraduate Research Program (CURP) in partnership with the National Society of Black Physicists (NSBP). ES, XC, MC, KM were supported from by the NYU Research Catalyst Prize. We thank anonymous reviewers for their feedback.